Arch Appl Mech (2020) 90:1547–1567
https://doi.org/10.1007/s00419-020-01683-6

ORIGINAL

K. Dragos · T. Makarios · I. Karetsou · G. D. Manolis · K. Smarsly

Detection and correction of synchronization-induced errors in operational modal analysis

Received: 6 November 2019 / Accepted: 14 February 2020 / Published online: 27 February 2020

Abstract Operational modal analysis (OMA) methods are frequently applied for obtaining information on structural dynamic parameters, such as natural frequencies and mode shapes. While synchronization between acceleration response data sets used in OMA is not a prerequisite for estimating natural frequencies, synchronization discrepancies may lead to non-negligible errors in the estimation of mode shapes. Synchronization discrepancies are predominantly associated with wireless structural health monitoring systems, where each wireless sensor node functions as a separate data acquisition unit (DAQ), and clock synchronization is therefore not intrinsic. However, synchronization discrepancies may also occur in cable-based systems, particularly when more than one DAQ is used. In this paper, a synchronization method for detecting and correcting synchronization-induced errors in OMA is proposed. Unlike existing approaches on removing synchronization-induced errors at the output stage, the method proposed herein yields synchronized structural response data at an intermediate stage of OMA. Specifically, time lags between acceleration response data sets are detected based on estimates of the mode shapes obtained either from preliminary structural analysis or from engineering judgment assuming classical damping. The applicability of the proposed method is verified through simulations of a multi-degree-of-freedom oscillator and validated through ambient vibration field tests on a pedestrian overpass bridge.

Keywords Synchronization · Structural health monitoring · Ambient vibrations · Pedestrian bridges · Operational modal analysis

1 Introduction

Over the past couple of decades, structural health monitoring (SHM) has been increasingly applied for gaining insights into the structural condition of civil infrastructure [1–3]. To describe the actual condition of monitored structures through estimating values for key structural parameters, system identification is frequently employed [4,5]. Moreover, since collecting structural dynamic response data from oscillating structures is common practice in SHM, several system identification methods focus on investigating the dynamic behavior of structures [6,7]. In this direction, operational modal analysis (OMA) methods have been drawing increasing attention, owing to the relatively low implementation cost and the negligible disturbance in the operation of structures [8,9]. OMA methods yield estimates for structural dynamic properties, such as natural frequencies, mode shapes, and damping ratios, of lightly damped structures through processing of structural dynamic

K. Dragos · K. Smarsly
Chair of Computing in Civil Engineering, Bauhaus University Weimar, Coudraystraße 7, 99423 Weimar, Germany

T. Makarios · I. Karetsou · G. D. Manolis (✉)
Laboratory for Experimental Mechanics, Department of Civil Engineering, Aristotle University, 54124 Thessaloníki, Greece
E-mail: gdm@civil.auth.gr

response data. Contrary to experimental modal analysis, which uses the input–output relationship for extracting structural dynamic properties, OMA typically builds upon output-only methods that have been widely employed for system identification and damage detection [10–13]. To extract structural dynamic parameter values, OMA methods are applied either directly to the raw structural dynamic response data (time-domain methods) or to structural dynamic response data transformed into the frequency domain (frequency-domain methods) via the fast Fourier transform (FFT) [14].

The accuracy of structural dynamic parameter values extracted with OMA depends on the quality of structural dynamic response data and on the preprocessing performed to remove spurious components attributed to external measurement factors, such as ambient noise. In addition, for obtaining accurate estimates of mode shapes, all structural dynamic response data sets must be synchronized. Synchronization discrepancies result in phase differences between structural dynamic response data sets, which, in turn, lead to erroneous mode shapes [15,16]. Synchronization discrepancies primarily affect wireless SHM systems [17]. In particular, wireless sensor nodes operate essentially as autonomous data acquisition units with no centralized server imposing global clock synchronization over the entire wireless sensor network [18]. Furthermore, while in cable-based systems a centralized data acquisition unit (DAQ) usually ensures absolute synchronization, it is not uncommon that multiple data acquisition units are installed in a structure, operating independently from each other. Thus, cable-based SHM systems may also be prone to synchronization discrepancies. For ensuring the highest possible accuracy in structural dynamic parameter values extracted by OMA methods, synchronization-induced errors must be detected and subsequently corrected.

The synchronization among structural dynamic response data sets, such as acceleration response data sets, and the impact of synchronization discrepancies on OMA results have been the focus of extensive research in the fields of computer science and experimental structural dynamics. Particularly for wireless sensor networks, most synchronization schemes proposed are based on clock offset and clock drifting. Thorough reviews on network synchronization schemes from a computer science perspective can be found in Youn, Sundararaman et al., and Ranganathan and Nygard [19–21]. A popular approach for achieving high-precision synchronization in both wireless and cable-based SHM systems is incorporating GPS transceivers into the data acquisition units. For example, Bojko et al. have presented a wireless sensor node prototype equipped with a GPS transceiver for absolute synchronization with other sensor nodes, resulting in accurate OMA results [22]. A similar approach has been presented by Dinçer et al. for monitoring bridges [23]. In terms of cable-based systems, GPS synchronization between separate data acquisition units has also been implemented. For example, case studies involving bridges, viaducts and monumental structures in Italy [24], a high-rise building in France [25], and a sports stadium in Portugal [26] have been reported. However, as argued in [18], using GPS transceivers has proven to be particularly power-consuming, and GPS operation might be adversely affected by weather conditions and poor satellite coverage [27]. Other synchronization approaches, associated solely with wireless sensor networks, are based on transmitting "beacon signals" by one sensor node, typically depicted as "master node," so as to synchronize the clocks of the rest of the wireless sensor nodes [28–30]. Although conceptually simple, the widespread adoption of the master node concept is hindered by shortcomings affecting the synchronization quality, such as non-deterministic message delivery delays in multi-hop networks [31], and by placing a significant burden on the cost-effectiveness of the monitoring strategy, e.g., by requiring out-of-band synchronization sources (GPS transceivers) to obtain the reference time for the master node [32].

Further research efforts on removing synchronization-induced errors from OMA results can also be found in the literature. For example, Maes et al. have presented an optimization method for synchronizing acceleration response data sets offline, by detecting potential time lags through minimizing the phase differences between the acceleration response data sets [33]. In their investigation of spectral characteristics of asynchronous acceleration response data, Zhu and Au have introduced a method for extracting mode shapes from the asynchronous data [34]. Specifically, Zhu and Au suggested extracting local mode shapes using the non-synchronized acceleration response data sets and imposing a common scaling to the modal force power spectral density derived from all sets. Brincker and Brandt have proposed the utilization of the cross-correlation between acceleration response data sets for synchronization, provided one vibration mode is dominant [35]. In the same direction, using the cross-correlation between acceleration and displacement response data sets for detecting time lags has been the subject of the work from Ferrari et al. [36]. Finally, synchronization approaches employing data fusion through multi-rate Kalman filters have also been reported for accommodating data collected at different sampling rates and for synchronizing heterogeneous data [37,38].

The aforementioned approaches either tackle synchronization problems during initializing SHM systems, assuming adequate networking technologies are implemented, or focus on removing synchronization-induced errors at the output stage by performing relatively computationally expensive post-processing. This paper

presents a synchronization method for detecting and correcting synchronization-induced errors in SHM systems. The scope of the synchronization method encompasses exclusively OMA-based objectives and does not cover non-modal-analysis SHM practices for damage detection such as wave-propagation-based methods. The synchronization method is based on the concept of "phase locking" occurring between synchronized data sets, as introduced in applications of biological physics by Rosenblum et al. [39]. Broadly speaking, phase locking refers to the adjustment of frequencies occurring between the responses of two weakly interacting, self-sustained oscillating systems, thus indicating synchronization between the systems. From a SHM viewpoint, structural responses are obtained from different locations in the same structure and, drawing from structural dynamics concepts, exhibit a similar frequency content. Hence, phase locking at frequency components dominating the structural responses should be present in synchronized structural response data sets, assuming the structural behavior is dominated by normal (real) modes. In the absence of synchronization, time lags between sets of acceleration response data are detected based on the expected relationships between phase angles at peaks in the FFT amplitude spectra corresponding to vibration modes, which, following the phase locking concept, should be constant. The expected relationships between the phase angles are derived either from engineering judgment or from preliminary analysis under an approximation typically adopted in OMA of damping being proportional to mass and stiffness, thus resulting in real modes [40]. Following the detection of time lags, the acceleration response data sets are shifted accordingly. The applicability of the synchronization method is verified through simulations of a multi-degree-of-freedom (DOF) oscillator and validated through field tests on a pedestrian highway overpass bridge. The results of the analyses demonstrate the ability of the proposed method to detect and correct synchronization-induced errors in OMA.

The paper is organized as follows: First, the mathematical background for detecting time lags through the phase difference between two sets of acceleration response data is presented. Next, the steps of the synchronization method are explained. Then, a series of numerical simulations using a discrete parameter model are performed for verifying the synchronization method, followed by validation tests on the pedestrian overpass bridge. Finally, the paper concludes with a summary and a discussion on future research.

2 Detection of time lags between acceleration response data sets

The mathematical background for detecting time lags between different structural dynamic response data sets (i.e., discretized signals) draws from the theory of signal processing. The synchronization method is generally applicable using any type of structural dynamic response data; for simplicity, in this paper the focus is placed on acceleration response data. Assume two acceleration response data sets, set i and set j, representing the responses of a single-DOF harmonic oscillator under sinusoidal excitation measured with different data acquisition units. The mathematical expressions governing the two sets over time t are given in Eqs. 1 and 2:

$$f_i(t) = A_i \sin(\omega t + \theta_i) \quad t = \eta \Delta t, \quad \eta \in \mathbb{N} \tag{1}$$

$$f_j(t) = A_j \sin\left(\omega t + \theta_j\right) \quad t = \eta \Delta t, \quad \eta \in \mathbb{N}. \tag{2}$$

In the above equations, f is the function representing an acceleration response data set, A is the amplitude of vibration, θ is the actual phase angle, and ω is the natural frequency. If the two sets are synchronized, θ_i is equal to θ_j. If set j is delayed with respect to set i by a time lag τ (Fig. 1), the time lag is related to the phase difference between functions $f_i(t)$ and $f_j(t)$ as follows:

$$f_j(t-\tau) = A_j \sin\left(\omega(t-\tau) + \theta_j\right) \Leftrightarrow f_j(t) = A_j \sin\left(\omega t + \tilde{\theta}_j\right), \quad \tilde{\theta}_j = \theta_j - \omega\tau \tag{3}$$

$$\theta_i = \theta_j \Leftrightarrow \tau = \frac{\theta_i - \tilde{\theta}_j}{\omega}. \tag{4}$$

Therefore, to compute the time lag τ, the phase angles from both acceleration response data sets are necessary. For obtaining estimates of the actual phase angles, functions $f_i(t)$ and $f_j(t)$ are discretized into two time series ($f_{n,i}$ and $f_{n,j}$) and the FFT is applied, as shown in the following:

$$F_\kappa(\omega) = \sum_{n=0}^{N-1} f_n \cdot e^{-2\pi i \kappa \frac{n}{N}} \quad \kappa \in [0, N] \quad N \in \mathbb{N} \quad \omega = 2\pi\kappa \big/ (N\Delta t). \tag{5}$$

In Eq. 5, F is the κth element of the FFT of an N-point time series f, which represents each acceleration response data set, and Δt is the time step. The argument of each complex FFT value, calculated in Eq. 6,

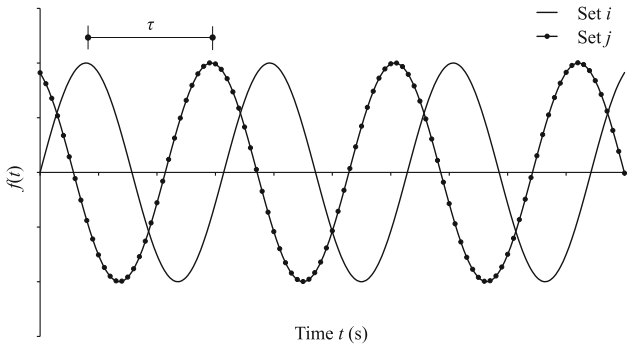

Fig. 1 Time lag between sets i and j of acceleration response data

corresponds to an estimate δ_o of the phase angle θ (i.e., the expected phase angle) of each harmonic function, namely the functions f_i and f_j of the structural response.

$$\delta_o(\omega_\kappa) = \arg(F_\kappa) = \arctan\left(\frac{\mathrm{Im}(F_\kappa)}{\mathrm{Re}(F_\kappa)}\right) \quad \kappa = \omega_\kappa \cdot \Delta t \cdot N. \tag{6}$$

The phase angle estimates derived from applying Eq. 6 with conventional computing processors lie within the interval $[0, 2\pi]$. Therefore, the maximum time lag that can be computed from Eq. 6 in a straightforward manner is:

$$\tau \leq \frac{\max\left(\delta_o(\omega_\kappa)_j - \delta_o(\omega_\kappa)_i\right)}{\omega} = \frac{2\pi}{\omega} = T \tag{7}$$

where T is the natural period of the oscillator. To extend Eq. 7 to account for time lags exceeding the natural period of the oscillator, the general trigonometric solution of Eq. 6 needs to be considered as follows:

$$\delta(\omega_\kappa) = \arctan\left(\frac{\mathrm{Im}(F_\kappa)}{\mathrm{Re}(F_\kappa)}\right)_{gen} = \delta_o(\omega_\kappa) + k\pi \quad k \in \mathbb{Z}. \tag{8}$$

By using Eq. 8, the general expression for estimating the time lag between two sets of acceleration response data is finally derived as:

$$\begin{aligned} \tau &= \frac{\delta(\omega_\kappa)_j - \delta(\omega_\kappa)_i}{\omega_\kappa} = \left(k_j - k_i\right)\frac{\pi}{\omega_\kappa} + \frac{\delta_o(\omega_\kappa)_j - \delta_o(\omega_\kappa)_i}{\omega_\kappa} \\ \Leftrightarrow \tau &= \tfrac{1}{2}T_\kappa b + \frac{\delta_o(\omega_\kappa)_j - \delta_o(\omega_\kappa)_i}{\omega_\kappa} \quad b = k_j - k_i \quad b, k_i, k_j \in \mathbb{Z}. \end{aligned} \tag{9}$$

Equation 9 can now be used as a basis for developing the time lag detection part of the proposed method, as described in the next section.

3 Detection and correction of synchronization-induced errors in OMA

In this section, the steps toward detecting time lags between acceleration response data sets and correcting synchronization-induced errors in OMA are explained. First, the basic principle governing the dynamic behavior of structures in terms of phase differences between different acceleration response data sets is analyzed. Then, the steps of the synchronization method are discussed.

3.1 Relationships of phase angles between different acceleration response data sets

The dynamic behavior of civil engineering structures can be described by the superposition of vibration modes of a multi-DOF numerical representation of the structures. Each mode is essentially a vector of physical oscillation functions $\mathbf{y}_r$ of r degrees of freedom with amplitudes $\mathbf{A}_r$ and phase angles $\boldsymbol{\theta}_r$. It has been proven that physical oscillation functions corresponding to a vibration mode are correlated [41]. Moreover, in conventional

OMA applications in civil engineering structures, due to damping forces being considerably lower than inertial forces and elastic forces, energy dissipation is usually represented by viscous damping [14]. In addition, while damping is an obscure and not fully investigated area in structural dynamics and actual damping is generally non-proportional, for conventional civil engineering structures with low damping and for low-energy OMA excitations, structural damping is frequently assumed proportional to structural mass and stiffness (proportional damping assumption), thus resulting in the dynamic behavior being described by normal (real) modes [42,43]. Therefore, depending on the position of each DOF in the mode shape with respect to the equilibrium position of the structure, the oscillation functions within $\mathbf{y}_r$ are either fully positively or fully negatively correlated. For example, between two degrees of freedom g and h, the correlation ρ for mode p is related to the phase difference $\Delta\theta$, as shown in the following:

$$\Delta\theta_p = \left|\theta_g - \theta_h\right|_p = \begin{cases} 0 & \text{for } \rho = 1 \\ \pi & \text{for } \rho = -1 \end{cases} \quad g, h \in [1, r] \quad g, h \in \mathbb{N}. \tag{10}$$

Time lags between acceleration response data sets from degrees of freedom g and h can be calculated using Eq. 9 considering any vibration mode. However, since the value of b cannot be determined in a straightforward way, Eq. 9 needs to be applied for m vibration modes, each having own half-period multiples b_p, yielding sets of time lags each containing m "candidate time lags." The set whose candidate time lags have the lowest variability, which is expressed through the standard deviation σ of the candidate time lags in the set, is selected as the final set of time lags, as shown in Eq. 11:

$$\begin{aligned} &\tau_{p,n} = \tfrac{1}{2} b_{p,n} T_p + \frac{\delta_o(\omega_p)_g - \delta_o(\omega_p)_h - \Delta\theta_p}{\omega_p} \\ &\boldsymbol{\tau} = \left[\, \tau_{1,n} \;\; \tau_{2,n} \;\cdots\; \tau_{m,n} \,\right] \equiv \sigma_n(\tau) \to \min \quad \tau \in \left[\tau_{1,n}, \tau_{m,n}\right] \\ &n \in [0, B] \quad B = \prod_{p=1}^{m} b_p \quad p \in [1, m] \quad b_p \in \mathbb{Z} \quad n \in \mathbb{N}. \end{aligned} \tag{11}$$

Theoretically, Eq. 11 should yield correct time lags, even when considering the lowest possible number of vibration modes ($m = 2$), regardless of the length of the time lags. The criterion for selecting the final set of time lags for $m = 2$ is, after some mathematical manipulation:

$$\begin{aligned} \sigma(\tau) &= \frac{\sqrt{2}}{2}(\tau_1 - \tau_2) \\ &= \frac{\sqrt{2}}{2}\left(\frac{1}{2} b_1 T_1 + \frac{\delta_o(\omega_1)_g - \delta_o(\omega_1)_h - \Delta\theta_1}{\omega_1} - \frac{1}{2} b_2 T_2 - \frac{\delta_o(\omega_2)_g - \delta_o(\omega_2)_h - \Delta\theta_2}{\omega_2}\right) \to \min. \end{aligned} \tag{12}$$

Depending on the phase angles as derived from the FFT, Eq. 12 may be fulfilled for several combinations of b_1 and b_2, thus resulting in several local minima. The global minimum of Eq. 12 corresponds to the correct set of time lags for acceleration response data sets perfectly sampled. However, deviations between the phase angles estimated via the FFT and the actual phase angles larger than 0.15–0.20 rad, due to spectral leakage or to interference from external factors, may compromise the accuracy of the time lags, thus increasing the risk of misinterpreting a local minimum as global minimum and of obtaining "false positive" time lag detections. To reduce the risk of false positives, it is recommended to account for the following:

- Boundaries for the longest possible time lags anticipated (both positive and negative depending on which acceleration data set is designated as reference set), i.e., limits to the potential time lags that are not expected to be exceeded in practice, should be defined. By defining these boundaries, the number of minima fulfilling Eq. 12 is reduced.
- For given limits of potential time lags, the number of candidate time lags depends on the periods T_1, T_2 of the vibration modes. As a result, for reducing the number of candidate time lags, and, by extension, the number of minima in Eq. 12, it is advised to use vibration modes with long periods.
- By setting $m > 2$, Eq. 12 may apply for more than one pairs of modes, thus reducing the number of candidate time lags to minima satisfying Eq. 12 for all pairs of modes. Nevertheless, it should be noted that increasing m may be detrimental to the computational efficiency.

The computational burden of calculating B sets of candidate time lags considering all possible combinations of time lags obtained from m modes increases significantly for large b_p values, which are necessary particularly for high-frequency modes. To enhance the efficiency of Eq. 11, a two-step process toward finding the set of time lags with minimum variability is suggested: First, one mode (prominent in the acceleration response data) is selected as the "dominant" mode according to which an initial candidate time lag τ_1 is calculated. Then, for each of the $m-1$ modes, only one candidate time lag is selected based on minimizing its difference to τ_1, thus eliminating $b_p - 1$ candidate time lags for each mode. As a result, the number of sets of candidate time lags is reduced to the half-period multiple of the dominant mode b_{dom}, from which the final set of time lags is selected, as shown in the following:

$$\begin{aligned}
&\tau_{1,n} = \tfrac{1}{2} b_{1,n} T_1 + \tfrac{\delta_o(\omega_1)_g - \delta_o(\omega_1)_h - \Delta\theta_1}{\omega_1} \\
&\boldsymbol{\nu} = \left[\, \tau_{2,n} \;\; \tau_{3,n} \;\cdots\; \tau_{m,n} \,\right] \equiv D = \left(\tfrac{1}{m-1} \sum_{p=2}^{m} \left| \tau_{1,n} - \tau_{p,n} \right| \right) \to \min \\
&\boldsymbol{\tau} = \left[\, \tau_{1,n} \;\; \boldsymbol{\nu} \,\right] \equiv \sigma_n(\tau_n) \to \min \quad \tau_n \in \left[\tau_{1,n}, \tau_{m,n} \right] \\
&n \in [0, b_{dom}] \quad p \in [2, m] \quad b_{dom} \in \mathbb{Z} \quad m, n \in \mathbb{N}.
\end{aligned} \tag{13}$$

To further reduce the probability of false positives, upon calculating $\boldsymbol{\tau}$, the time lags are cross-validated by synchronizing acceleration response data sets g and h according to $\boldsymbol{\tau}$ and by obtaining the phase angles φ_g and φ_h at q vibration modes (with $q > m$) using the FFT. To accept the set of time lags $\boldsymbol{\tau}$, the difference between $(\varphi_g - \varphi_h)$ and $\Delta\theta$ for all q vibration modes must be lower than a threshold value ε, which is case-specifically defined based on the precision of the acceleration response data, as shown in Eq. 14.

$$\varphi_{c,g} - \varphi_{c,h} - \Delta\theta < \varepsilon \quad c \in [1, q] \quad q \in \mathbb{N}. \tag{14}$$

Equation 13, hereinafter termed "phase shift condition," will be used as a basis for the method proposed in this paper, the steps of which are explained in the following subsection.

3.2 Description of the synchronization method

Assuming a lightly damped structure instrumented with a SHM system measuring the structural response at r degrees of freedom, the steps followed toward detecting and correcting synchronization-induced errors in OMA are outlined in the flowchart of Fig. 2. The application of the synchronization method is divided into two parts: (a) preliminary analysis, in case of either first application of the synchronization method or if changes in the structural state have occurred and (b) main analysis if the structural state, and, by extension, the expected phase differences $\Delta\theta$ for all vibration modes considered are known.

The *preliminary analysis* includes the following steps:

1. A numerical model of the structure is created for obtaining estimates of the expected natural frequencies $\boldsymbol{\omega}_e = \{\omega_{e1}, \omega_{e2}, \ldots, \omega_{em}\}$ and of the expected mode shapes $\boldsymbol{\Phi}_e = \{\boldsymbol{\varphi}_{e1}, \boldsymbol{\varphi}_{e2}, \ldots, \boldsymbol{\varphi}_{em}\}$, focusing on the degrees of freedom actually measured. Since this step is only associated with defining expected phase differences, the numerical model is generally kept simple in terms of discretization. However, gross simplifications that could affect the ability of the numerical model to adequately describe the dynamic behavior of the structure should be avoided to limit the exposure of the results of the synchronization method to epistemic uncertainty. Furthermore, when applying the synchronization method to long-term SHM systems, large variations in structural properties (e.g., mass variations due to traffic or changing weather conditions) that could significantly affect the structural dynamic parameters need to be taken into account and be reflected in the computation of the expected mode shapes. It should be noted that small deviations between expected natural frequencies and experimentally extracted natural frequencies (step 2) do not affect the synchronization method, since the expected phase differences depend on the relative positions of discretized lumped mass, which are usually insensitive to small changes in frequency. Finally, in cases where the expected dynamic behavior of the structure can be inferred from engineering judgment, the numerical model may be unnecessary.
2. Sets of acceleration response data are collected to obtain m peaks in the Fourier amplitude spectrum corresponding to vibration modes (modal peaks). From the modal peaks, m experimental values of the natural frequencies $\boldsymbol{\omega} = \{\omega_1, \omega_2, \ldots, \omega_m\}$ are derived.

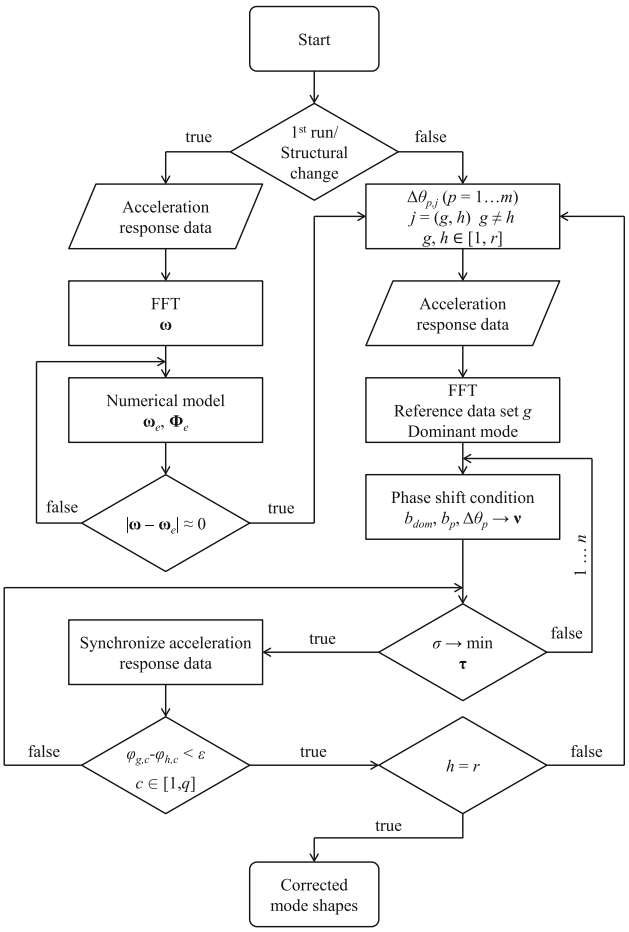

Fig. 2 Flowchart with the steps of the synchronization method

3. If there are discrepancies between the experimental natural frequencies and the expected natural frequencies, the numerical model is updated accordingly.
4. The expected phase differences $\Delta\theta_1 \ldots \Delta\theta_m$ are obtained for each pair of degrees of freedom considered using the corresponding expected mode shapes.

The *main analysis* is performed as follows:

1. Acceleration response data sets are derived from all measured degrees of freedom and transformed into the frequency domain via FFT.
2. One acceleration response data set is selected as reference, according to which the rest of the acceleration response data sets are synchronized, and one modal peak is selected as the dominant mode.
3. The phase shift condition (Eq. 13) is applied for r data sets, for m vibration modes, for predefined values of b_{dom} and b_p $(p = 2 \ldots m)$, and for given limits of potential time lags.
4. Upon deriving the estimates of the time lags, the acceleration response data sets are accordingly shifted.
5. The accuracy in detecting the time lags is cross-validated for q vibration modes using the acceleration response data sets shifted in step 4.
6. Modal identification is conducted for extracting the mode shapes from the synchronized acceleration response data sets, which are then compared to the expected mode shapes.

It should be emphasized that the fundamental requirement of the proposed synchronization method is that damping can be reasonably approximated as proportional to structural mass and stiffness. For structures where the proportional damping assumption does not hold, the applicability of the proposed synchronization method is not guaranteed. Furthermore, the synchronization method is not intended to restore absolute synchronization between data acquisition units, which would require time lag detection precision in the order of microseconds; rather, the objective of the proposed method is to accurately reproduce mode shapes. Hence, the precision

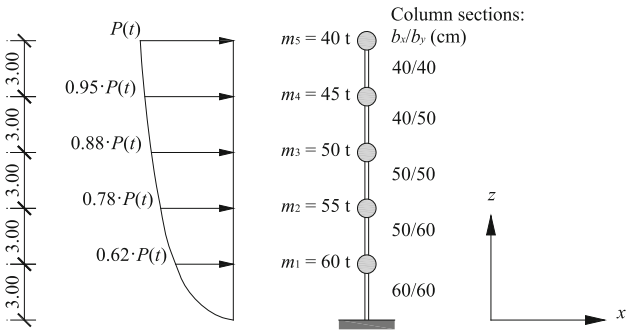

Fig. 3 Five-DOF oscillator simulation for the verification tests

tolerance of time lag detection could be reasonably set to a few milliseconds, resembling discrepancies expected due to the approximate nature of the FFT in estimating phase angles and to external factors interfering with the acceleration response data. This tolerance level is expected to have minimal effect on mode shapes of interest in conventional civil engineering structures, whose natural frequencies usually do not exceed 15 Hz. For modes at high frequencies, the accuracy in time lag detection may be compromised.

4 Verification through simulations using a multi-degree-of-freedom oscillator

In this section, the proposed synchronization method is verified through simulations of a multi-DOF oscillator, which is essentially a discrete parameter numerical model of a steel cantilever. The purpose of the verification tests is to investigate the applicability of the synchronization method in cases where the time lags are artificially inserted and are therefore known a priori. First, the numerical model is mathematically described and then results from applying the synchronization method are presented.

4.1 Description of the multi-degree-of-freedom oscillator numerical model

The numerical model of the oscillator comprises five lumped masses, as depicted in Fig. 3. The structural vibration response is assumed to follow the "stick model" paradigm, i.e., only the five translational degrees of freedom (u_1–u_5) in the horizontal (X) direction are taken into account.

The numerical model is analyzed under broadband Gaussian excitation, using a load distribution profile in compliance with wind-induced excitations as specified in Eurocode 1 [44], assuming terrain category I, basic wind speed $v_b = 25$ m/s, air density $\rho_a = 1.25\,\mathrm{kg/m^3}$, and orography factor $c_o = 1$. The sets of simulated acceleration response data from the oscillator are derived through a time-history analysis. A total of 65,536 data points are collected for each set at a sampling rate of 1000 Hz. To perform the time-history analysis, the Newmark-β algorithm is applied [45], with the expansions for the velocities and accelerations given in Eq. 15, by setting the values of the algorithm parameters to $\gamma = 0.5$ and $\beta = 0.25$.

$$\begin{aligned} \dot{x}_{n+1} &= \dot{x}_n + (1-\gamma)\cdot\Delta t\cdot\ddot{x}_n + \gamma\cdot\Delta t\cdot\ddot{x}_{n+1} \\ x_{n+1} &= x_n + \dot{x}_n\cdot\Delta t + 1/2\cdot(\Delta t)^2\cdot\left[(1-2\beta)\cdot\ddot{x}_n + 2\beta\cdot\ddot{x}_{n+1}\right]. \end{aligned} \tag{15}$$

In Eq. 15, $\ddot{x}$, $\dot{x}$, and x are the nth acceleration, velocity, and displacement response data point, respectively.

4.2 Results from the verification tests

The first verification test (test 1) aims at proving the applicability of the synchronization method for different lengths of time lags. To this end, synchronization discrepancies are inserted into the acceleration response data sets ranging from $\tau_{\min} = -1$ s to $\tau_{\max} = 1$ s at a step of $\Delta\tau = 0.001$ s. All possible pairs of acceleration response data sets are considered. For applying the phase shift condition (Eq. 13), a combination of modes per pair of acceleration response data sets needs to be defined based on the modal peaks at the corresponding Fourier amplitude spectra illustrated in Fig. 4. The frequencies and periods of the modal peaks derived from

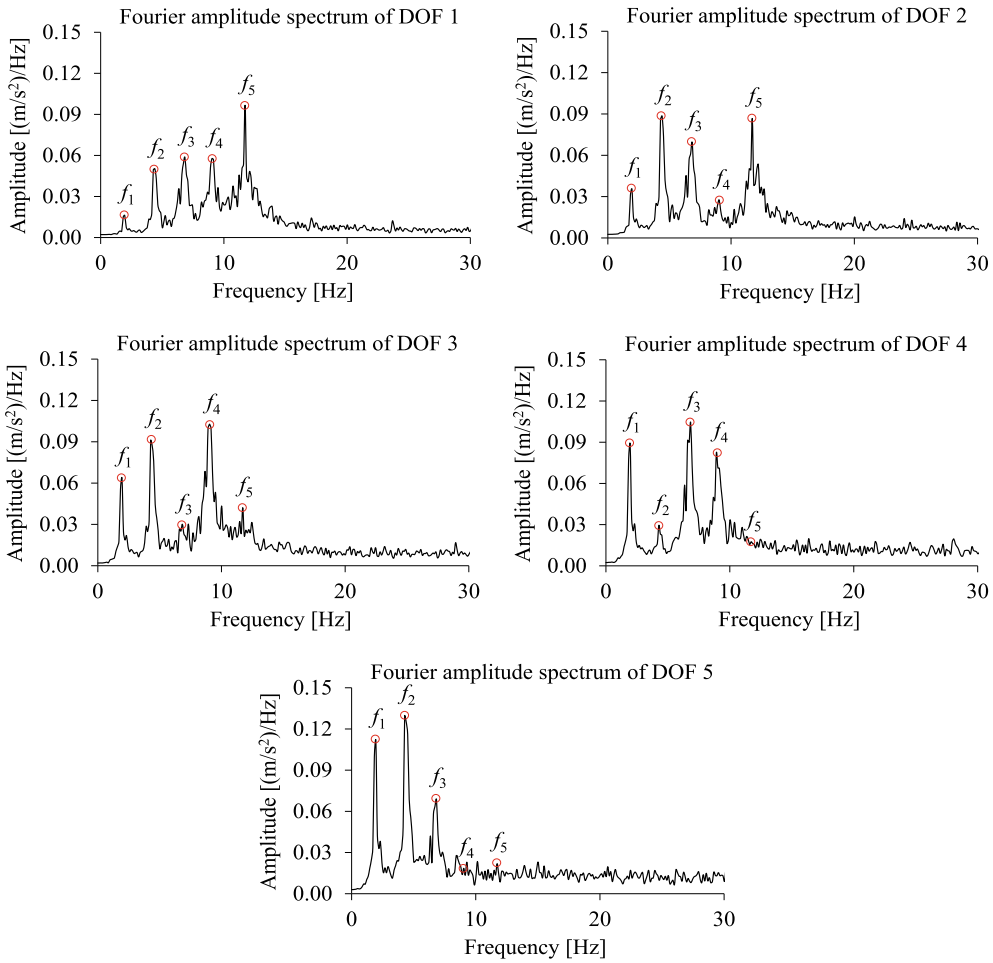

Fig. 4 Fourier amplitude spectra of all degrees of freedom of the oscillator

Table 1 Frequencies and periods of the oscillator

Mode	FFT		Modal analysis	
	Frequency (Hz)	Period (s)	Frequency (Hz)	Period (s)
1	1.953	0.512	1.914	0.522
2	4.395	0.228	4.416	0.226
3	6.744	0.148	6.693	0.149
4	8.911	0.112	9.056	0.110
5	11.749	0.085	11.752	0.085

FFT are presented in Table 1, including the frequencies and periods of the numerical model calculated through modal analysis for comparison purposes.

As shown in Fig. 4, the level of excitation among the degrees of freedom varies at different frequencies. Low amplitudes in the Fourier amplitude spectrum may indicate degrees of freedom being close to nodal (i.e., zero-crossing) points in the corresponding mode shapes. Modal peaks with amplitudes that are not easily discernible in the spectrum are deemed not suitable for calculating phase shifts, as the calculations may be affected by the relatively high contribution of spurious noise frequency components infiltrating the structural response data. Therefore, for each pair of acceleration response data sets, the combination of modal peaks should be carefully selected so that the corresponding amplitudes are adequately large in both data sets. For keeping the computational load as low as possible, the number of vibration modes for applying the phase shift condition is set equal to $m = 2$ for all pairs of acceleration response data sets.

Table 2 Combinations of vibration modes for cross-validation

Data set	1	2	3	4	5
1	N/A	f_1-f_2-f_3-f_5	f_1-f_2-f_4-f_5	f_1-f_2-f_3-f_4	f_1-f_2-f_3
2	Symmetric	N/A	f_1-f_2-f_4	f_1-f_2-f_3	f_1-f_2-f_3
3			N/A	f_1-f_2-f_4	f_1-f_2-f_3
4				N/A	f_1-f_2-f_3
5					N/A

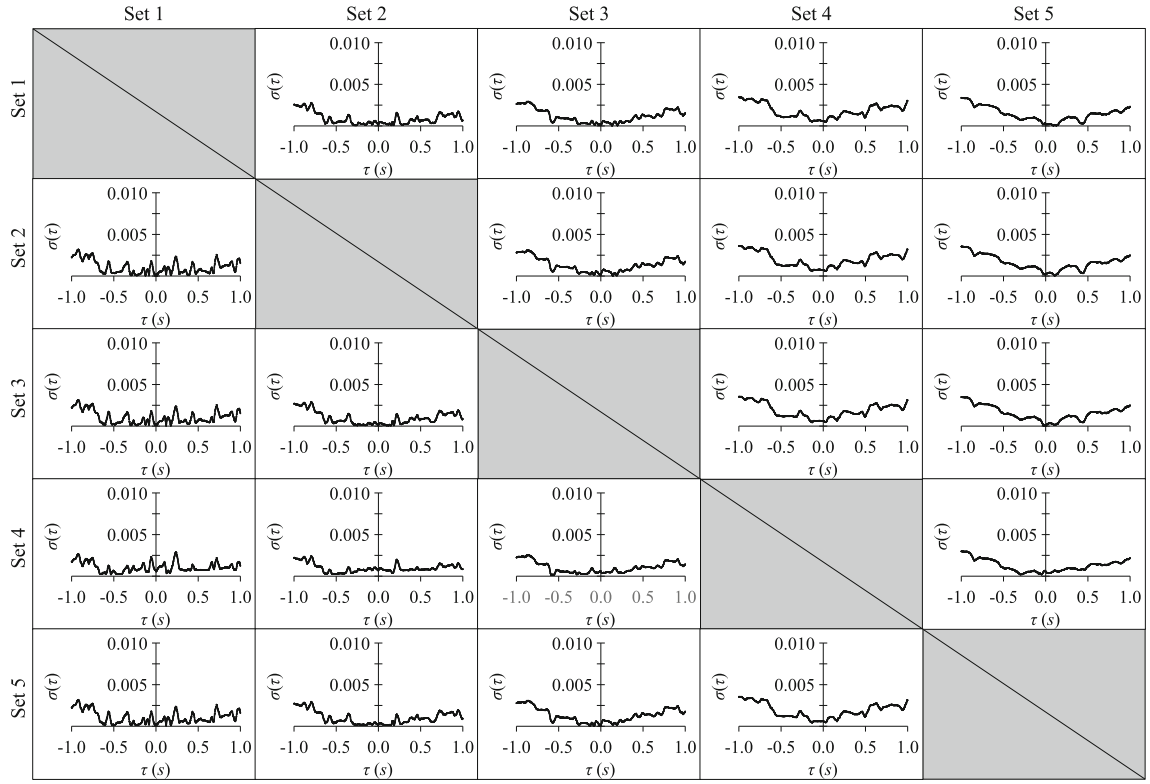

Fig. 5 Standard deviations from applying the phase shift condition for all pairs of acceleration data sets over the entire range of artificially inserted time lags

Furthermore, to reduce the probability of false positives, the phase shift condition is applied for all pairs using the first two vibration modes, which have the longest periods and which are adequately excited in all acceleration response data sets. For the cross-validation tests, q is selected separately for each pair of acceleration response data sets based on the level of excitation of the modal peaks, as shown in Fig. 4. The limits for potential time lags for the purposes of the test are set equal to 2.0 s for positive time lags and − 2.0 s for negative time lags, respectively; despite the low likelihood of long time lags occurring in state-of-the-art SHM systems, the limits are deliberately exaggerated in the test to prove the validity of the proposed synchronization method even for long time lags. Finally, the threshold value ε is set equal to 0.10 rad. The combinations of vibration modes for the cross-validation are shown in Table 2.

The results from applying the synchronization method for all pairs of acceleration response data sets are shown in Fig. 5. Specifically, the standard deviations σ as calculated from the phase shift condition (Eq. 13) are plotted against the time lags τ that are artificially inserted into the second acceleration response data set of each pair, which is depicted in the horizontal axis. According to the phase shift condition (Eq. 13), convergence of all elements in vector $\boldsymbol{\tau}$ to the same time lag is showcased by minimizing the standard deviation of these elements, which in turn indicates that the phase shift condition has yielded a reliable estimate of the actual time lag. In this verification test, the time lag τ is a priori known, since it is artificially inserted, and is included in vector $\boldsymbol{\tau}$ for calculating the standard deviation:

Table 3 Time lags inserted and detected into the acceleration response data sets

DOF	Inserted time lag (ms)	Detected time lag (ms)	
		τ_1	τ_2
1	Ref.	N/A	N/A
2	−21	−21	−20.2
3	187	187	187.5
4	8	9	8
5	−113	−112.3	−114.1

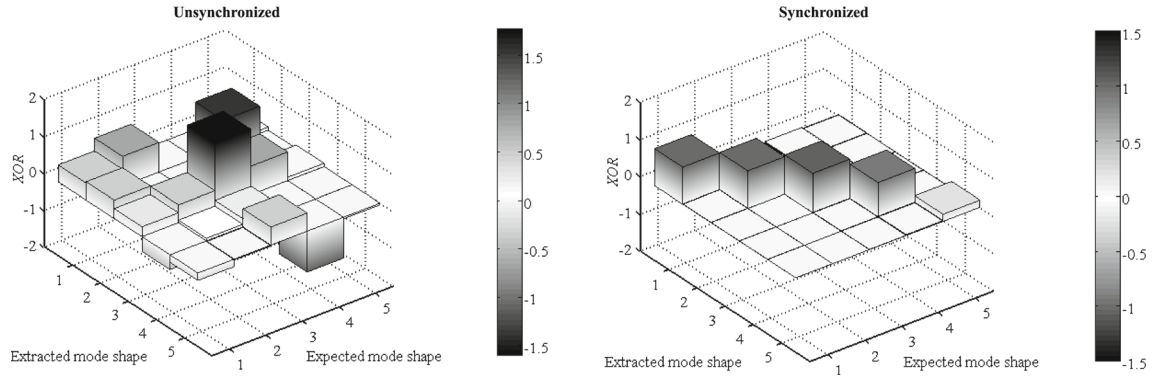

Fig. 6 XOR plots of the mode shapes before and after applying the synchronization method

$$\boldsymbol{\tau} = \left[\tau \;\; \tau_{1,n} \;\; \boldsymbol{\nu}\right] \equiv \sigma_n\left(\tau_n\right) \rightarrow \min \quad \tau_n \in \left[\tau, \tau_{1,n} \cdots \tau_{m,n}\right]. \tag{16}$$

As a result, and only for this verification test, the standard deviation serves a twofold purpose: (i) To prove that candidate time lags extracted using the phase shift condition converge to the same time lag and (ii) confirm the reliability of the estimate to which candidate time lags converge by proving its proximity to the actual (artificially inserted) time lag. From preliminary analyses, it has been observed that a standard deviation of $\sigma < 0.005$ is indicative of convergence.

To showcase the favorable effect of the synchronization method in correcting mode shapes, another test is conducted (test 2) by inserting one set of time lags to the acceleration response data sets of the cantilever structure. The objective of test 2 is to extract mode shapes before and after applying the synchronization method and to compare the respective mode shapes to the expected mode shapes derived from modal analysis. A comparison is performed using the cross-orthogonality check (XOR), which describes the orthogonality between the expected mode shapes $\boldsymbol{\Phi}_w$ and the experimental mode shapes $\boldsymbol{\Psi}_v$ weighted with respect to the mass matrix $\mathbf{M}_w$ of the numerical model [46]:

$$\mathrm{XOR}\left(\boldsymbol{\Phi}_w, \boldsymbol{\Psi}_v\right) = \boldsymbol{\Phi}_w^T \cdot \mathbf{M}_w \cdot \boldsymbol{\Psi}_v. \tag{17}$$

If the acceleration response data sets are synchronized, the similarity between the extracted mode shapes and the expected mode shapes is anticipated to be high and is expressed by XOR ≥ 0.9 for $w = v$ and XOR ≤ 0.1 for $w \neq v$, provided that both mode matrices $\boldsymbol{\Phi}_w$, $\boldsymbol{\Psi}_v$ are mass-normalized. The time lags inserted into the acceleration response data sets along with the time lags detected by applying the synchronization method are summarized in Table 3. Parameters m, q and ε, as well as the combinations of modes, are selected equal to the corresponding values of test 1. No time lag has been inserted into the acceleration response data set of DOF u_1, which is assigned as reference data set. The mode shapes before and after applying the synchronization method (i.e., "unsynchronized and "synchronized," respectively) are extracted via a modal identification algorithm using the frequency-domain decomposition method [47] and normalized to DOF u_5. The XOR values for all modes are shown in Fig. 6. The mode vectors are presented in Table 4, and the respective mode shapes are illustrated in Fig. 7.

The results of the verification tests clearly prove the ability of the proposed method to detect and to correct synchronization-induced errors in the OMA results. The agreement between the extracted mode shapes and the expected mode shapes is more prominent in the first four vibration modes. In the fifth mode, while applying the phase shift condition has removed the synchronization-induced errors in the extracted mode shape, there

Table 4 Modal vectors before and after applying the synchronization method

DOF	Mode				
	1	2	3	4	5
	$f = 1.953$ Hz	$f = 4.395$ Hz	$f = 6.744$ Hz	$f = 8.911$ Hz	$f = 11.749$ Hz
Unsynchronized					
u_1	0.0800	0.3760	2.4470	− 5.9650	4.8150
u_2	0.2420	0.6630	1.3290	0.0830	13.6920
u_3	− 0.5720	0.4960	− 0.0630	− 15.1520	6.4970
u_4	0.3450	0.1670	− 3.8150	− 9.6200	0.9320
u_5	1.0000	1.0000	1.0000	1.0000	1.0000
Synchronized					
u_1	0.1460	− 0.3740	1.1370	− 2.5900	11.3210
u_2	0.3140	− 0.6570	1.3560	− 0.9340	− 11.1590
u_3	0.5510	− 0.6830	− 0.2900	4.9210	5.5600
u_4	0.7620	− 0.1860	− 1.7630	− 3.3120	− 0.7790
u_5	1.0000	1.0000	1.0000	1.0000	1.0000
Expected					
u_1	0.1508	− 0.3719	1.0397	− 2.9170	60.5960
u_2	0.3191	− 0.6523	1.2222	− 0.9466	− 58.0795
u_3	0.5595	− 0.6753	− 0.3916	5.0672	24.6026
u_4	0.7783	− 0.1796	− 1.7103	− 3.9613	− 7.3444
u_5	1.0000	1.0000	1.0000	1.0000	1.0000

are deviations between the extracted mode shape and the expected mode shape in the amplitudes of the masses. These deviations may be attributed to the low level of excitation of the respective vibration mode and to DOF u_5 (used as a mode shape normalization reference) being close to a zero-crossing point in the fifth mode, thus exhibiting low oscillation amplitude at the respective frequency. As a result of the low oscillation amplitude, the modal peak of u_5 at the fifth mode may be contaminated with spurious frequency content, which affects the accuracy of the modal identification algorithm, as reflected in the respective XOR plots. While the verification tests prove the applicability of the synchronization method, further tests using real acceleration response data from a field case study are necessary for validating the method.

5 Validation tests on a pedestrian overpass bridge

To validate the synchronization method using measured acceleration response data, a case study on a pedestrian highway overpass bridge instrumented with two independently operating, and thus unsynchronized, cable-based SHM systems, is conducted. First, from the pedestrian bridge structural and architectural blueprints, information on the structural properties is obtained. This information is used for performing numerical simulations of the bridge to recover the expected natural frequencies and the corresponding mode shapes required for validating the proposed synchronization method. Then, an outline of the instrumentation scheme with the two SHM systems is presented, and the ambient vibration tests are described. Finally, the results from applying the proposed method are discussed.

5.1 Description of the bridge

The pedestrian overpass bridge shown in Fig. 8 facilitates pedestrian traffic over the Inner-Ring highway road in Thessaloniki, Greece, and is one of two overpass bridges located in the municipality of Evosmos, to the west of Thessaloniki. The bridge spans 40.80 m in length and its deck width is 5.35 m, resting on two 80-cm-diameter cylindrical reinforced concrete columns at each end, as shown in Fig. 8. The deck is a composite structure comprising a corrugated steel trough filled with concrete. In the longitudinal direction, the deck is supported by two steel girders running along its edges. The deck girders rest on the column heads, which have spherical base isolation bearings acting as load transferring interfaces.

In the transverse direction, the deck rests on 20 equidistant beams, which are welded to the main girders. There are ten x-braces, each spanning two consecutive beam openings, for a total of 20 brace elements with an overlap at the center. Past the column supports, the deck continues and abuts two lateral stairways, one at

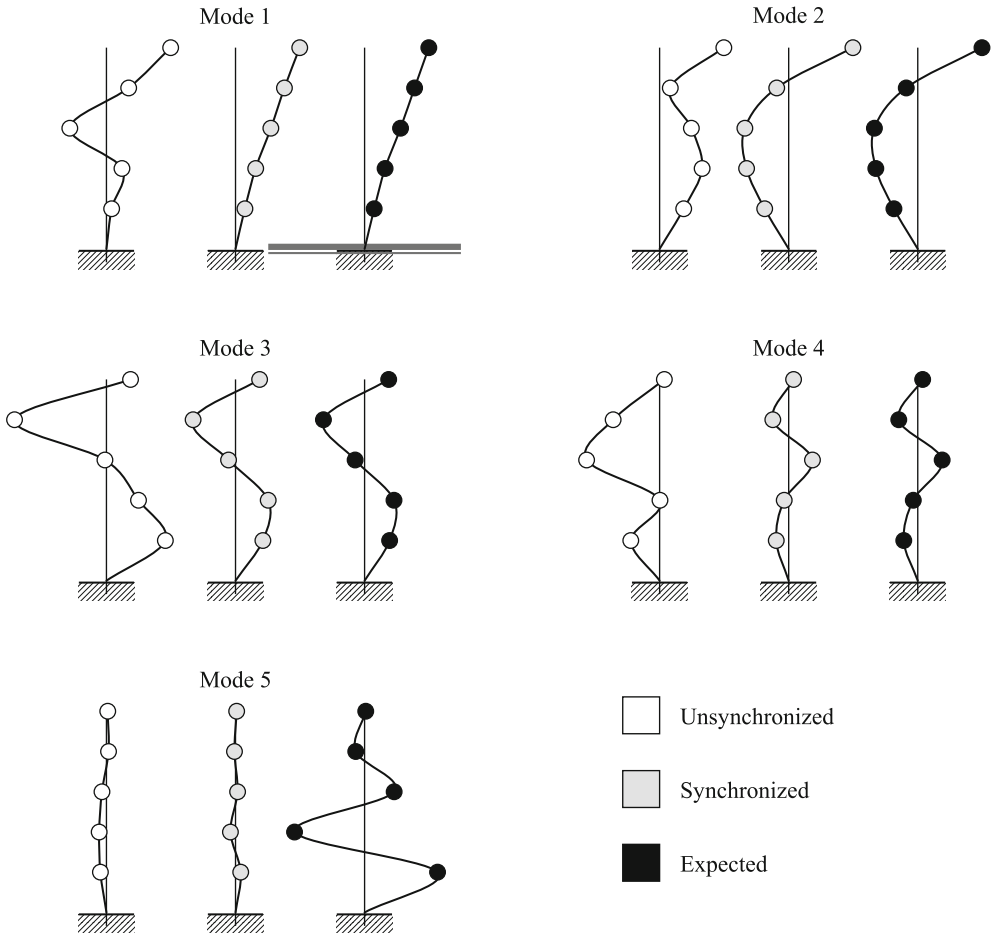

Fig. 7 Mode shapes before and after applying the synchronization method

Fig. 8 The pedestrian highway overpass bridge

each end, as shown in Fig. 9. The bracing system also continues past the column supports with one additional x-brace at each end. The x-braces add to the lateral stiffness of the bridge, as shown in Fig. 8. Furthermore, the vertical support of the bridge provided by the main girders is complemented by two skewed steel arches, from which the deck is suspended through 16 steel twisted strand cables along each longitudinal edge of the deck. The arches are connected to each other in the transverse direction at three points, namely the mid-span and the quarter-length points from each end. As shown in Fig. 8, each arch end rests directly on top of one column. According to the structural details, which are confirmed by visual inspection, the bridge deck support conditions on one end can be modeled as hinges, while at the other end as rollers.

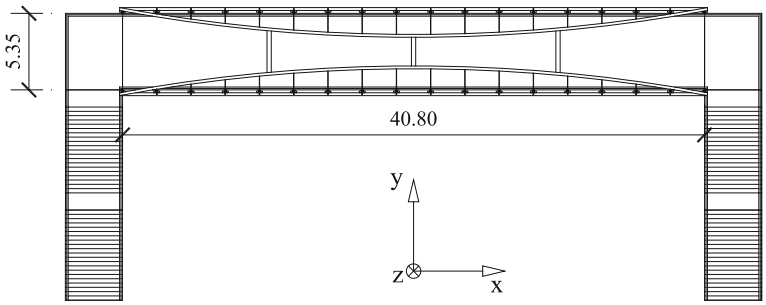

Fig. 9 Plan view of the pedestrian bridge with two stairways at the ends

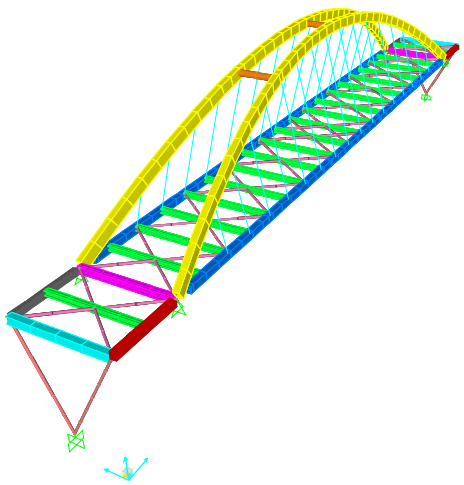

Fig. 10 3D view of the FE model of the overpass pedestrian bridge

5.2 Numerical modeling of the pedestrian bridge

The entire bridge, except the two stairways at the ends of the bridge deck that are practically self-standing and with minimal lateral support from the bridge itself, is modeled using the finite element (FE) analysis commercial package SAP 2000 [48]. The purpose of the numerical modeling is to retrieve the expected mode shapes that will be used for applying the phase shift condition. Two-point linear (beam) elements combining bending, axial, and torsional behavior are used for modeling the bridge structural elements. The elasticity modulus of the steel elements is $E_s = 210\,\text{GPa}$, while the elasticity modulus of the twisted strand cables is $E_{cab} = 1653\,\text{GPa}$. The mass density of steel is taken as equal to $7.85 \times 10^3\,\text{kg/m}^3$. Furthermore, the deck and the railings are also taken into account as adding to the overall bridge stiffness and mass.

A 3D view of the numerical model is shown in Fig. 10. The expected mode shapes are obtained by performing modal analysis using the numerical model. This numerical model is subjected to minor calibrations to assure adequate convergence between the expected natural frequencies and experimental natural frequencies obtained as part of the "preliminary analysis." Due to the complexity of the structure and the use of several materials, the minor calibrations do not aim to optimize global material parameters, such as moduli of elasticity. Rather, the minor calibrations primarily focus on simply approximating the deck-to-column connections, whose fixity, as previously mentioned, ranges from a hinge to a roller due to the presence of the interface bearings. As a result, the FE model is fine-tuned using the natural frequencies obtained from the preliminary (experimental) analysis to give an accurate representation of the current structural state of the overpass bridge. The accuracy of the FE model is deemed adequate for obtaining the expected phase differences; as previously mentioned, the numerical model as part of preliminary analysis is generally kept simple, albeit avoiding gross simplifications that may result in erroneously estimating the relative position of discretized masses in the mode shapes.

The results from performing modal analysis using the numerical model of the pedestrian bridge are shown in Fig. 11. Since the instrumentation is limited to the bridge deck, modes describing primarily the oscillation of the arches are neglected.

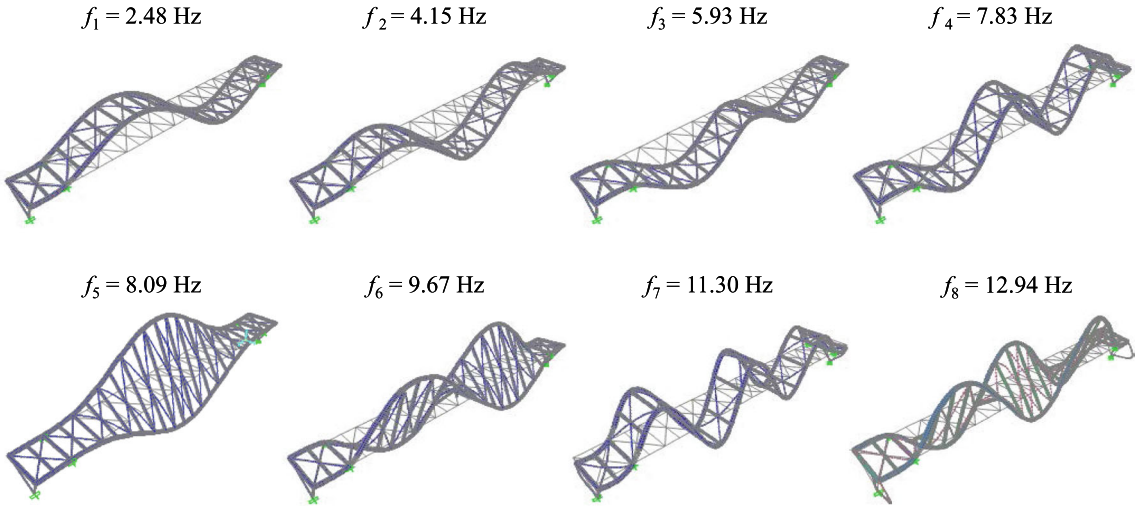

Fig. 11 Results of modal analysis using the FE model of the bridge

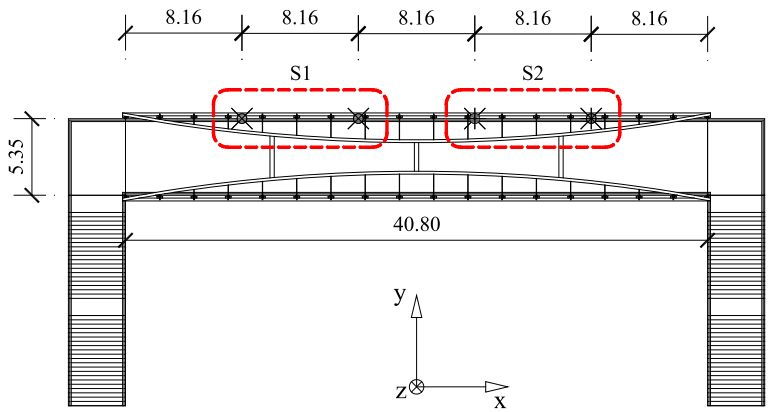

Fig. 12 Bridge instrumentation layout

5.3 Description of the SHM instrumentation and of the ambient vibration tests

The bridge is instrumented with two structural health monitoring systems, labeled as S1 and S2. Since the objective of the test is to validate the ability of the synchronization method to detect time lags between two SHM systems, modal identification and, by extension, the instrumentation are kept as simple as possible. SHM system S1 consists of two KYOWA-ASW-2A accelerometers and a KYOWA PCD-300A DAQ [49,50], and SHM system S2 consists of two PCB 393A03 accelerometers [51] and a National Instruments NI USB-6002 DAQ [52]. As shown in Fig. 11, the dynamic behavior of the bridge is expected to comprise a combination of translational vibration modes in the Z direction and torsional vibration modes about the longitudinal axis of the deck. Given the simple instrumentation used, the focus is placed on the translational vibration modes. The sensors are equally spaced at 8.16 m locations from each other, i.e., at the 1/5 points along the total span length. The bridge instrumentation is shown in Fig. 12. The bridge is newly constructed at the time the measurements are conducted and is, therefore, closed to pedestrian traffic. Thus, the acceleration response data are collected from ambient vibrations caused by the heavy traffic moving under the bridge, including a large number of trucks, and by the crew of eight graduate students and two faculty members conducting the measurements.

For applying the synchronization method, four acceleration response data sets, corresponding to the four instrumented locations on the bridge deck, are collected at a sampling rate of 512 Hz for a duration of 10 min under operational conditions (i.e., vehicular traffic under the bridge and simulated pedestrian traffic by the crew conducting the measurements). The data sets are averaged using a window of 32,768 points and 50% overlap to enhance the signal-to-noise ratio. In this case study, the data acquisition units of SHM system S1 and SHM system S2 operate independently from each other, thus resulting in synchronization-induced errors. Therefore,

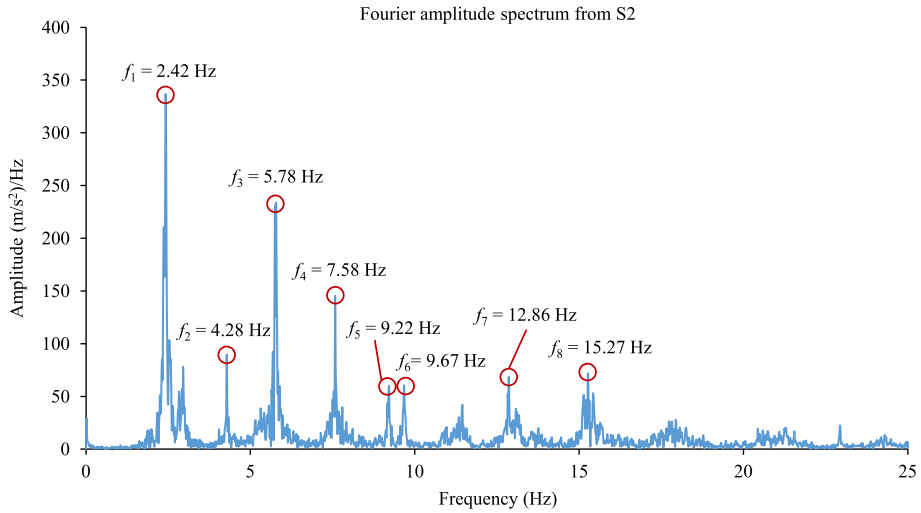

Fig. 13 Fourier amplitude spectrum from the preliminary analysis (SHM system S2)

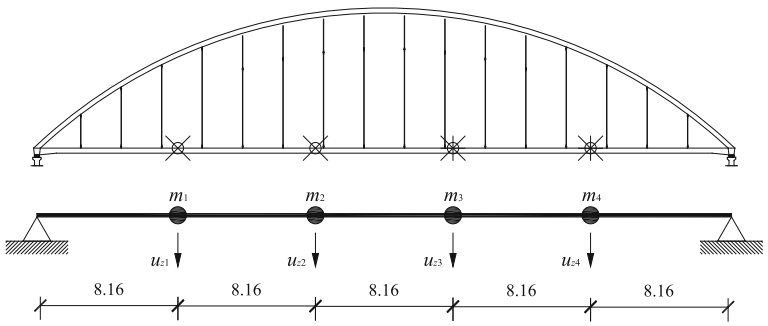

Fig. 14 Four-DOF beam model of the bridge deck for modal identification

no synchronization discrepancies between the two sets of acceleration response data collected from each SHM system are expected. Instead, an overall time lag between the SHM systems should be observed, due to the non-simultaneous initialization of the SHM systems. First, the modal peaks identified from the preliminary analysis, the Fourier amplitude spectrum of which is plotted in Fig. 13, and the modal analysis results of the FE model are used for computing the expected phase differences $\Delta\theta_1 \ldots \Delta\theta_m$.

Modal identification in this case study is performed using the frequency-domain decomposition method, as in test 2 of the verification tests, which is applied both before and after applying the synchronization method (unsynchronized and synchronized modes, respectively). For defining the expected mode shapes, a beam model of the bridge deck is created with four degrees of freedom corresponding to the instrumented locations of the deck. The purpose of reducing the FE model to a four-DOF beam model is twofold: (1) to obtain the expected phase differences and (2) to facilitate the comparison between the experimental mode shapes and the numerical mode shapes. All degrees of freedom are in the vertical (Z) direction, as illustrated in Fig. 14. DOF u_{z1} is set as reference and the sets of acceleration response data at degrees of freedom u_{z2}, u_{z3}, and u_{z4} are synchronized according to the reference. The first two vibration modes are considered ($m = 2$) as being the modes with the highest contribution to the overall bridge dynamic response and with the longest periods. For cross-validation, the number of vibration modes is set equal to $q = 4$ with the combination f_1–f_2–f_3–f_4 selected as the combination of modes exhibiting the highest amplitudes in the Fourier amplitude spectrum and ε is set equal to 0.10 rad. The limits for detectable time lags are set equal to 2.0 s and -2.0 s, respectively. The estimated time lags are summarized in Table 5.

As anticipated, for DOF u_{z2} the time lag detected is negligible for the purposes of the synchronization method; therefore, acceleration response data sets u_{z1} and u_{z2} are synchronized. For u_{z3} and u_{z4}, a small, yet non-negligible, variability between the time lags detected from the first and the second vibration mode is observed. Since this variability appears to be practically constant in both acceleration response data sets, it is

Table 5 Time lags detected in the validation test

	DOF			
	u_{z1}	u_{z2}	u_{z3}	u_{z4}
τ_1 (s) ($f = 2.42$ Hz)	N/A	0.002	− 1.335	− 1.334
τ_2 (s) ($f = 4.28$ Hz)	N/A	− 0.001	− 1.348	− 1.350

Table 6 Time lags detected in the validation test

	DOF			
	u_{z1}	u_{z2}	u_{z3}	u_{z4}
τ_1 (s) ($f = 2.42$ Hz)	N/A	0.002	− 1.335	− 1.334
τ_2 (s) ($f = 4.28$ Hz)	N/A	− 0.001	− 1.348	− 1.350
τ_3 (s) ($f = 5.78$ Hz)	N/A	0.001	− 1.344	1.345

Table 7 Modal vectors before and after applying the synchronization method

DOF	Mode			
	1 $f = 2.42$ Hz	2 $f = 4.28$ Hz	3 $f = 5.78$ Hz	4 $f = 7.58$ Hz
Unsynchronized				
u_{z1}	0.7590	− 1.3640	− 0.6870	− 1.6790
u_{z2}	0.5240	5.6540	− 0.2760	3.0940
u_{z3}	0.6750	− 3.9080	0.2760	− 1.3570
u_{z4}	1.0000	1.0000	1.0000	1.0000
Synchronized				
u_{z1}	− 0.9540	0.9910	0.9280	− 1.2880
u_{z2}	− 0.6800	− 4.1820	0.3480	2.3650
u_{z3}	0.6830	− 4.1740	0.2780	− 1.3880
u_{z4}	1.0000	1.0000	1.0000	1.0000
Expected				
u_{z1}	− 0.9794	1.2673	1.0650	− 0.8040
u_{z2}	− 0.7108	− 4.4593	0.2702	1.3711
u_{z3}	0.6772	− 4.1970	0.3731	− 1.4355
u_{z4}	1.0000	1.0000	1.0000	1.0000

attributed to deviations between the phase angles computed by the FFT and the actual phase angles, e.g., due to approximations. As a result, the analysis is repeated by setting $m = 3$ and including f_3 in the phase shift condition. The results from repeating the analysis are presented in Table 6.

From Table 6, it is observed that the time lags detected for vibration mode f_3 are closer to the time lags detected for vibration mode f_2. Since mode f_3 has a shorter period and is expected to be more sensitive to small time lag deviations, all acceleration response data sets are synchronized according to the time lags detected for mode f_3. From the modal analysis results of the numerical model (Fig. 11), it is evident that the fifth translational mode (f_7) has four nodal points, which, given the relative symmetry of the bridge structural system, are expected to coincide with the instrumentation points. As a result, the current setup is deemed suitable for detecting only the first four translational modes (f_1, f_2, f_3, f_4). The mode vectors before and after applying the synchronization method are presented in Table 7, and the corresponding mode shapes are shown in Fig. 15. Following the same process as in verification test 2, the XOR plots before and after applying the synchronization method are illustrated in Fig. 16.

From the results of the validation tests, it is clear that the synchronization method yields accurate estimates of mode shapes. Moreover, the effect of synchronization-induced errors appears to be weaker on the fourth mode; this could be attributed to the time lag being close to a false positive local minimum for the fourth mode. The mode shape after applying the phase shift condition is, nonetheless, closer to the respective expected mode shape. Despite the lack of strong convergence to a single time lag value, the favorable effect of the synchronization method is apparent in the corrected mode shapes. Moreover, it is evident that the accuracy of the synchronization method in detecting time lags depends on the accuracy of the phase angles detected via the FFT. It is therefore recommended to obtain long acceleration response data sets, which can be averaged

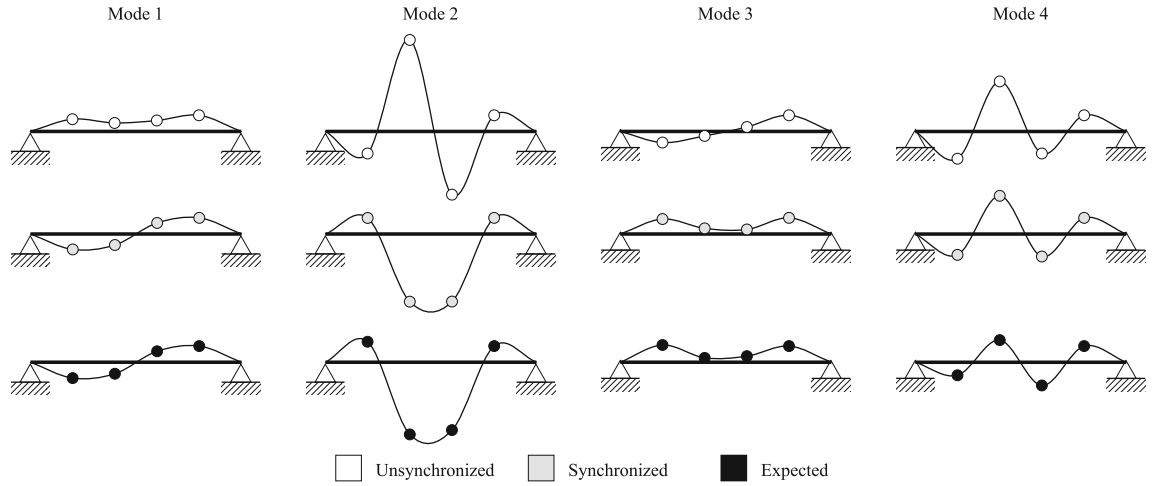

Fig. 15 Mode shapes before and after applying the synchronization method

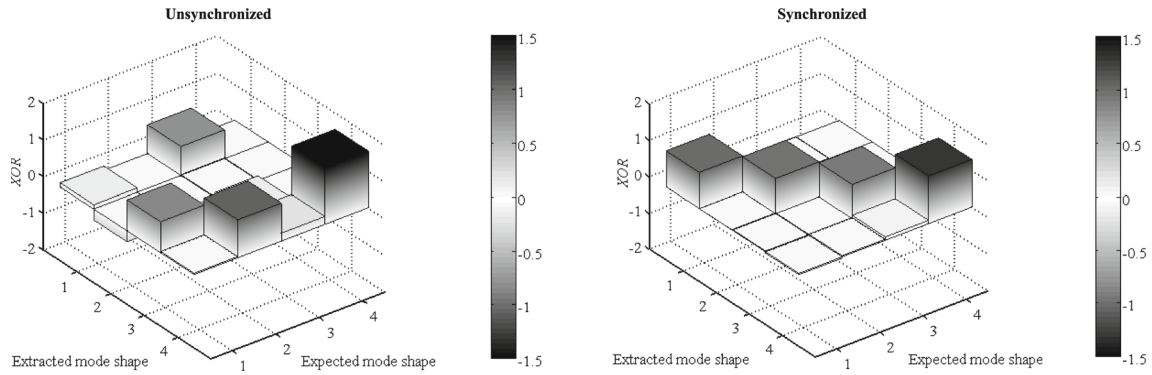

Fig. 16 XOR plots before and after applying the synchronization method

to eliminate the effects of ambient noise, and to keep the discretization of the Fourier amplitude spectra dense enough to compensate for sampling effects on the Fourier transform, such as spectral leakage. Finally, it should be noted that the validation test presented above serves as proof-of-concept through a real-world case study. Adopting the proposed synchronization method on a broad scale requires accounting for a series of factors that are likely to affect the quality of the time lag estimation, thus raising the need for defining the applicability limits of the method. Examples of potential challenges include:

- Deriving reliable estimates of the expected phase differences from numerical analysis in cases of gradual (aging) or rapid (loss of stationarity) changes in the structural dynamic properties, e.g., crowd concentrations on decks of lightweight pedestrian bridges or structural degradation due to damage.
- Correctly identifying pairs of expected and experimental natural frequencies in cases of large modal density and closely spaced modes.
- Handling complex modes and distinguishing between phase differences attributed to mode complexity from phase differences caused by lack of synchronization, even in cases where the experimentally extracted modes are near-real [53].
- Evaluating the sensitivity of the time lag estimation to SHM instrumentation parameters, such as sampling rate, noise floor, and window size.

The aforementioned challenges constitute critical considerations for adopting the synchronization method in actual SHM practice and are largely associated with the monitoring objectives and the type of structure to be monitored. A study on the applicability limits of the synchronization method, accounting for the aforementioned challenges, will be the topic of future work by the authors.

6 Summary and conclusions

Structural health monitoring is being widely applied nowadays for maintaining civil engineering infrastructure. In this context, system identification serves as a methodology for extracting information on important structural parameters of the structure in question. In system identification, operational modal analysis for deriving structural dynamic parameters of monitored structures, such as natural frequencies and mode shapes, has been gaining increasing popularity. In OMA, synchronization discrepancies between acceleration response data sets compromise the accuracy in evaluating structural dynamic parameters. More specifically, phase differences between sets of acceleration response data, as a result of synchronization discrepancies, lead to erroneous mode shapes. While synchronization discrepancies predominantly affect wireless SHM systems, cable-based systems with more than one data acquisition units may also be prone to synchronization-induced errors. Research efforts for removing synchronization-induced errors from OMA results focus on either implementing clock synchronization technologies or using computationally intensive optimization methods at the output stage of OMA. In this work, a synchronization method for detecting and correcting synchronization-induced errors in OMA at an intermediate stage of the analysis has been presented. In the proposed method, acceleration response data are first transformed into the frequency domain via FFT. Using the expected relationships between phase angles of frequency components corresponding to vibration modes under the assumption of classical damping, time lags between acceleration response data sets are detected. Finally, the acceleration response data sets are synchronized according to the time lags.

The applicability of the synchronization method has been verified through numerical simulations of the response of a multi-degree-of-freedom oscillator. The results of the verification tests have demonstrated the ability of the synchronization method to detect accurate time lags and yield correct mode shapes. It has also been observed that the accuracy in detecting time lags is affected by the number of modes considered for applying the phase shift condition and by the level of excitation of the modal peaks. Next, a validation field test has been conducted on a pedestrian overpass bridge to further demonstrate that the synchronization method can accurately reproduce mode shapes using acceleration response data from actual SHM systems. Good quality results have been obtained from the validation tests. Time lags between the acceleration response data sets have been successfully detected, and the mode shapes extracted using OMA have been corrected. When applying the proposed method, special attention should be paid to avoiding false positives corresponding to local minima satisfying the equations used to compute time lags. To avoid erroneous estimates of time lags, it is recommended to collect long acceleration response data sets to ensure high accuracy in computing phase angles through the FFT. Future work will be directed toward implementing the proposed method using other types of structural dynamic response data. Furthermore, the quality of the results produced by the proposed method will be further investigated and quantified on a statistical basis, also considering the existence of complex mode shapes.

Acknowledgements The authors gratefully acknowledge the support offered by the German Research Foundation (DFG) under Grant SM 281/14-1 for the initiation of the German–Greek collaboration. We would also like to acknowledge the support offered by DFG through the research training group GRK 1462 entitled "Evaluation of Coupled Numerical and Experimental Partial Models in Structural Engineering." The valuable assistance provided by Dr. Panayiotis Panetsos, project manager at Egnatia Odos S.A., in making the pedestrian overpass bridge available for ambient vibration measurements is also acknowledged. Finally, the authors also wish to acknowledge the financial support provided by the Thuringian Ministry for Economic Affairs, Science and Digital Society (TMWWDG) and the Open Access Publication Funds of Bauhaus University Weimar. Major parts of this work were conducted in the "Structural Health Monitoring Laboratory," sponsored by the European Union through the European Fund for Regional Development (EFRD) and TMWWDG under Grant 2016 FGI 0009. Any opinions, findings, conclusions, or recommendations expressed in this paper are those of the authors and do not necessarily reflect the views of the sponsors.

References

1. Adams, D.E.: Health Monitoring of Structural Materials and Components: Methods with Applications. Wiley, Hoboken (2007)
2. Farrar, C.R., Worden, K.: Structural Health Monitoring: A Machine Learning Perspective. Wiley, Hoboken (2012)
3. Smarsly, K., Hartmann, D., Law, K.H.: An integrated monitoring system for life-cycle management of wind turbines. Int. J. Smart Struct. Syst. **12**(2), 209–233 (2013)
4. Peeters, B.: System identification and damage detection in civil engineering structures. Ph.D. Dissertation, KU Leuven, Leuven, Belgium (2000)
5. Smarsly, K., Hartmann, D., Law, K.H.: A computational framework for life-cycle management of wind turbines incorporating structural health monitoring. Struct. Health Monit. Int. J. **12**(4), 359–376 (2013)

6. Saisi, A., Gentile, C., Guidobaldi, M.: Post-earthquake continuous dynamic monitoring of the Gabbia Tower in Mantua, Italy. Constr. Build. Mater. **81**, 101–112 (2015)
7. Dragos, K., Smarsly, K.: A hybrid system identification methodology for wireless structural health monitoring systems based on dynamic substructuring. In: Proceedings of the SPIE Smart Structures/NDE Conference: Sensors and Smart Structures Technologies for Civil, Mechanical, and Aerospace Systems, Las Vegas, NV, USA, 24/03/2016 (2016)
8. Zhang, L., Brincker, R., Andersen, P.: An overview of operational modal analysis: major development and issues. In: Proceedings of the 1st International Operational Modal Analysis Conference, Copenhagen, Denmark, 26/04/2005 (2005)
9. Ubertini, F., Comanducci, G., Cavalagli, N., Laura Pisello, A., Luigi Materazzi, A., Cotana, F.: Environmental effects on natural frequencies of the San Pietro bell tower in Perugia, Italy, and their removal for structural performance assessment. Mech. Syst. Signal Process. **82**, 307–322 (2017)
10. Magalhães, F., Cunha, Á., Caetano, E.: Vibration based structural health monitoring of an arch bridge: from automated OMA to damage detection. Mech. Syst. Signal Process. **28**, 212–228 (2012)
11. Comanducci, G., Magalhães, F., Ubertini, F., Cunha, Á.: On vibration-based damage detection by multivariate statistical techniques: application to a long-span arch bridge. Struct. Health Monit. **15**(5), 505–524 (2016)
12. Deraemaeker, A., Reynders, E., De Roeck, G., Kullaa, J.: Vibration-based structural health monitoring using output-only measurements under changing environment. Mech. Syst. Signal Process. **22**(1), 34–56 (2008)
13. Ubertini, F., Comanducci, G., Cavalagli, N.: Vibration-based structural health monitoring of a historic bell-tower using output-only measurements and multivariate statistical analysis. Struct. Health Monit. **15**(4), 438–457 (2016)
14. Brincker, R., Ventura, C.: Introduction to Operation Modal Analysis. Wiley, Chichester (2015)
15. Krishnamurthy, V., Fowler, K., Sazonov, E.: The effect of time synchronization of wireless sensors on the modal analysis of structures. Smart Mater. Struct. **17**(5), 055018 (2008)
16. García-Palacios, J., Tirando-Andrés, E., Soria, J.M., Díaz, I.M., Araujo, Á.: Effects of time synchronization on operational modal analysis. In: Proceedings of the 6th International Operational Modal Analysis Conference, Gijón, Spain, 12/05/2015 (2015)
17. Rainieri, C., Fabbrocino, G.: Operational Modal Analysis of Civil Engineering Structures: An Introduction and Guide for Applications. Springer, New York (2014)
18. Smarsly, K., Law, K.H., König, M.: Autonomous structural condition monitoring based on dynamic code migration and cooperative information processing in wireless sensor networks. In: Proceedings of the 8th International Workshop on Structural Health Monitoring, Stanford, CA, USA, 09/13/2011 (2011)
19. Youn, S.: A comparison of clock synchronization in wireless sensor networks. Int. J. Distrib. Sensor Netw. 2013, ID532986 (2013)
20. Sundararaman, B., Buy, U., Kshemkalyani, A.D.: Clock synchronization for wireless sensor networks: a survey. Ad-Hoc Netw. **3**(3), 281–323 (2005)
21. Ranganathan, P., Nygard, K.: Time synchronization in wireless sensor networks: a survey. Int. J. UbiComp **1**(2), 92–102 (2010)
22. Bojko, T., Lisowski, W., Bednarz, J.: Problems of development of wireless sensors for experimental modal analysis. Diagnostyka **3**(51), 49–58 (2009)
23. Dinçer, S., Aydin, E., Gencer, H.: A real-time instrumentation approach for structural health monitoring of bridges. In: Proceedings of the Istanbul Bridge Conference, Istanbul, Turkey, 11/08/2014 (2014)
24. Peeters, B., Sforza, G., Sbaraglia, L., Germano, F.: Efficient operational modal testing and analysis for design verification and restoration baseline assessment: Italian case studies. In: Proceedings of the 4th International Conference on Experimental Vibration Analysis for Civil Engineering Structures, Varenna, Italy, 03/10/2011 (2011)
25. Fernández-Lorenzo, G. W., Mercerat, D., Santisi d'Avila, M. P., Bertrand, E., Deschamps, A.: Operational modal analysis of a highrise RC building and modelling. In: Proceedings of the 6th International Operational Modal Analysis Conference, Gijón, Spain, 12/05/2015 (2015)
26. Magalhães, F., Caetano, E., Cunha, Á.: Operational modal analysis of the Braga sports stadium suspended roof. In: Proceedings of the 24th International Modal Analysis Conference, St. Louis, MO, USA, 02/02/2006 (2006)
27. Wang, L., Xu, Q.: GPS-free localization algorithm for wireless sensor networks. Sensors **10**(2010), 5899–5926 (2010)
28. Whelan, M.J., Gangone, M.V., Janoyan, K.D., Jha, R.: Real-time wireless vibration monitoring for operational modal analysis of an integral abutment highway bridge. Eng. Struct. **31**(10), 2224–2235 (2009)
29. Van Greunen, J., Rabaey, J.: Lightweight time synchronization for sensor networks. In: Proceedings of the 2nd ACM International Conference on Wireless Sensor Networks and Applications, San Diego, CA, USA, 19/09/2003 (2003)
30. Severino, R., Gomes, R., Alves, M., Sousa, P., Tovar, E., Ramos, L.F., Aguilar, R., Lourenço, P.B.: A wireless sensor network platform for structural health monitoring: enabling accurate and synchronized measurements through COTS+ custom-based design. In: Proceedings of the 5th Conference on Management and Control of Production and Logistics, Coimbra, Portugal, 08/09/2010 (2010)
31. Maggs, M.K., O'Keefe, S.G., Thiel, D.V.: Consensus clock synchronization for wireless sensor networks. IEEE Sens. **12**(6), 2267–2277 (2012)
32. Stojmenovic, I.: Handbook of Sensor Networks. Algorithms and Architectures. Wiley, Hoboken (2005)
33. Maes, K., Reynders, E., Rezayat, A., De Roeck, G., Lombaert, G.: Offline synchronization of data acquisition systems using system identification. J. Sound Vib. **381**, 264–272 (2016)
34. Zhu, Y.-C., Au, S.-K.: Spectral characteristics of asynchronous data in operational modal analysis. Struct. Control Health Monit. 2017, e1981 (2017)
35. Brincker, R., Brandt, A.: Time synchronization by modal correlation. In: Proceedings of the 4th International Operational Modal Analysis Conference, Istanbul, Turkey, 09/05/2011 (2011)
36. Ferrari, R., Pioldi, F., Rizzi, E., Gentile, C., Chatzi, E. N., Serantoni, E., Wieser A.: Fusion of wireless and non-contact technologies for the dynamic testing of a historic RC bridge. Meas. Sci. Technol. 27(12), 124014 (2016)

37. Chatzi, E., Fuggini, C.: Structural identification of a super-tall tower by GPS and accelerometer data fusion using a multi-rate Kalman filter. In: Proceedings of the 3rd International Symposium on Life-Cycle Civil Engineering (IALCCE 2012), Vienna, Austria, 03/10/2012 (2012)
38. Smyth, A., Wu, M.: Multi-rate Kalman filtering for the data fusion of displacement and acceleration response measurements in dynamic system monitoring. Mech. Syst. Signal Process. **21**(2), 706–723 (2007)
39. Rosenblum, M., Pikovsky, A., Kurths, J., Schäfer, G., Tass, P.A.: Phase synchronization: from theory to data analysis. In: Moss, F., Gielen, S. (eds.) Handbook of Biological Physics, vol. 4, pp. 279–321. Elsevier, Amsterdam (2001)
40. Ibrahim, S.R.: Existence and normalization of complex modes in post experimental use in modal analysis. In: Silva, J.M.M., Maia, N.M.M. (eds.) Modal Analysis and Testing, pp. 441–452. Kluwer Academic Publishers, Dordrecht (1999)
41. Dragos, K., Smarsly, K.: Distributed adaptive diagnosis of sensor faults using structural response data. Smart Mater. Struct. 25(10), 105019 (2016)
42. Liang, Z., Lee, C.G.: Damping of structures: part 1—theory of complex damping. Technical Report NCEER-91-0004. National Center for Earthquake Engineering Research, State University of New York, Buffalo, NY, USA (1991)
43. Caughey, T.K., O'Kelly, M.E.J.: Classical normal modes in damped linear dynamic systems. J. Appl. Mech. **32**(3), 583–588 (1965)
44. STN EN-1991: Eurocode 1: Actions on structures. Part 1–4: general actions—wind actions. European Institute for Standardization (CEN), Brussels (2010)
45. Newmark, N.M.: A method of computation for structural dynamics. ASCE J. Eng. Mech. **85**(3), 67–94 (1959)
46. Skafte, A., Aenlle, M.L., Brincker, R.: Cross orthogonality check for structures with closely spaced modes. In: Proceedings of the 33rd International Modal Analysis Conference, Orlando, FL, USA, 02/02/2015 (2015)
47. Brincker, R., Zhang, L.: Frequency domain decomposition revisited. In: Proceedings of the 3rd International Operational Modal Analysis Conference, Portonovo, Italy, 04/05/2009 (2009)
48. Computers and Structures, Inc.: SAP 2000 Integrated Finite Element Analysis and Design of Structures: Version 19. Computers and Structures, Inc., Berkeley (2013)
49. KYOWA: ASW-A Waterproof Acceleration Transducer Specification Sheet. KYOWA Electronic Instruments, Ltd., Tokyo (2017)
50. KYOWA: PCD 300A Sensor Interface Specification Sheet. KYOWA Electronic Instruments, Ltd., Tokyo (2004)
51. PCB Piezotronics Vibration Division: Seismic ICP Accelerometer (Model Number: 393A03) Specification Sheet. PCB Group Inc, Depew (2008)
52. Instruments, National: NI USB-6002 DAQ Device Specification Sheet. National Instruments Corporation, Austin (2014)
53. Brandt, A.: Noise and Vibration Analysis. Signal Analysis and Experimental Procedures. Wiley, Chichester (2011)